Energy Conversion and Management 361 (2026) 121622

Contents lists available at ScienceDirect

Energy Conversion and Management

journal homepage: www.elsevier.com/locate/enconman

Research Paper

From case-specific to general tuning: A structured, system-level framework for scalable RCCI simulation

Kian Golbaghi [a,*], Hamidreza Maleki Almani [a,b], Alireza Kakoee [a], Ben Smulter [c], Jari Hyvönen [c], Amin Andwari [d], Maciej Mikulski [a]

[a] Efficient Powertrain Solutions (EPS), School of Technology and Innovation, University of Vaasa, Wolffintie 32, FI-65200 Vaasa, Finland
[b] Department of Mathematics and Statistics, School of Technology and Innovation, University of Vaasa, Wolffintie 32, FI-65200 Vaasa, Finland
[c] Engine Research and Technology Development at Wärtsilä Marine Solutions, Vaasa, Finland
[d] Machine and Vehicle Design (MVD), Materials and Mechanical Engineering, Faculty of Technology, University of Oulu FI-90014 Oulu, Finland

ARTICLE INFO

Keywords:
Dual-fuel engine
RCCI
Predictive combustion models
Multi-zone model
Engine calibration

ABSTRACT

Multi-zone models (MZMs) are widely used for system-level simulation of reactivity-controlled compression ignition (RCCI) engines. However, their predictive robustness remains strongly dependent on CFD-informed fuel stratification inputs, case-specific calibration and fuel-dependent chemical kinetic mechanisms. This limits their transferability across engine platforms and operating conditions. This study addresses these limitations by developing a structured, CFD-independent reduced-order predictive framework for scalable engine-level RCCI simulation. Implemented within the University of Vaasa's advanced thermo-kinetic multi-zone model (UVATZ), the methodology integrates (i) systematic reactivity scaling to compensate for chemical kinetic deficiencies without disturbing thermodynamic boundary conditions, and (ii) a generalised beta-distribution-based high-reactivity fuel stratification model which eliminates reliance on CFD-derived mixture profiles. The framework is encapsulated in a modular solver architecture and uses a structured calibration procedure requiring only limited test-bench data to achieve predictive capability. The new submodels were assessed for scalability across different chemical kinetic mechanisms, and their physical consistency was verified against CFD spray simulations. The complete framework was experimentally validated using 40 operating points from a prototype Wärtsilä W31 medium-speed dual-fuel engine operating in RCCI mode. Key performance metrics (maximum pressure and indicated mean effective pressure) were predicted within ± 6%, without case-specific tuning. CA50 errors were below 5 CAD (±1 CAD standard deviation). Model deviations remained within measured cycle-to-cycle variability, and simulation time did not exceed three minutes per cycle, comparing favourably against best-in-class multi-zone models which rely on calibration to a specific operating point.

1. Introduction

The maritime industry is a major source of emissions, so shifting to green fuels is essential to reduce greenhouse gas emissions (GHG) and meet increasingly strict international standards. This boosts demand for multi-fuel capability, and alternative fuels like hydrogen, ammonia and biofuels are expected to dominate the market in the coming decades [1], necessitating flexible propulsion systems [2]. Low-temperature combustion (LTC) technology presents a promising solution in this context, because it can operate with multiple fuel types and contribute to meeting the International Maritime Organisation's (IMO) Tier III regulations by minimising oxides of nitrogen (NOx) emissions and methane leakage [3,4]. Reactivity-controlled compression ignition (RCCI) through in-cylinder blending of two fuels has recently gained significant attention, particularly in large-bore engines and the maritime sector [5–7]. The key feature of RCCI engines is a premixed charge of low-reactivity fuel (LRF) and direct cylinder injection of a high-reactivity fuel (HRF) [8,9]. This process provides superior control over the heat release rate through in-cylinder reactivity stratification and, more recently, with variable valve actuation (VVA)-enabled thermal management [10].

The engine characteristics in LTC are highly sensitive to fuel injection strategies and fuel properties [11]. Many researchers have explored engine designs and control strategies for various fuel combinations. Premkumar et al. [12] used direct numerical simulation (DNS) to investigate ignition phenomena in n-octanol/ethanol RCCI

* Corresponding author.

https://doi.org/10.1016/j.enconman.2026.121622
Received 9 March 2026; Received in revised form 8 May 2026; Accepted 10 May 2026
Available online 16 May 2026

configurations. They coupled a 2D flow solver and a detailed chemistry solver to reveal the co-existence of deflagration and spontaneous ignition fronts. They demonstrated the sensitivity of combustion behaviour to the initial scalar field distributions. Using high-fidelity CFD tools, Halis et al. [13] investigated the effects of intake manifold pressure, premixed fuel ratio and intake air temperature on RCCI performance. This study highlighted the difficulty of controlling combustion phasing solely by adjusting the premixed ratio, underscoring the need for more advanced modelling frameworks.

RCCI experiments further highlight the need for reliable simulation tools to address the difficulties in precisely controlling the fuel injection timing and premixing strategies, which are crucial for stable combustion and avoiding issues such as knocking [14]. The complex interplay between fuel injection timing, chamber thermodynamics and reactivity gradients makes accurate modelling difficult [15]. Yadav et al. [16] conducted optical spray investigations to calibrate numerical spray models for RCCI using ethanol and diesel. They found that even minor variations in the chamber temperature could drastically alter the ignition delay and combustion onset, emphasising the sensitivity of RCCI to the initial conditions. Additionally, RCCI operation (and consequently its simulation) is highly affected by the boundary conditions, particularly the thermal stratification caused by cylinder heat transfer [17].

There have been numerous attempts to develop a low-fidelity predictive model for studying the complex phenomena of RCCI. Zhou et al. [18] tried to develop a reduced-order model based on the Kiva4 CFD framework and Chemkin libraries. They developed flame propagation and two chemical submodels to synthesise two simulation approaches that proved to work well separately for homogeneous charge compression ignition (HCCI) and conventional diesel combustion (CDC). They showed that this integration could effectively cover the insufficiency of the Chemkin solver in predicting the combustion of certain dual-fuel conditions. In contrast, Franken et al. [19] applied stochastic reactor models (SRM) to heavy-duty RCCI engines, achieving accurate predictions of combustion phasing and emissions across varying operating conditions. SRMs methodological strength lies in its ability to incorporate complex reaction mechanisms, while maintaining a low computational cost by simulating combustion as an ensemble of statistically distributed reactor elements governed by detailed chemical kinetics. However, its zero-dimensional nature precludes spatial resolution, thereby limiting its applicability in modelling stratified reactivity fields and localised ignition phenomena.

As suggested by the literature, combustion modelling approaches for low-temperature and dual-fuel engine concepts vary widely in fidelity and computational cost. They range from high-resolution CFD to empirical and control-oriented models. CFD-based methods provide detailed insights into in-cylinder flow, spray evolution, and the interaction between turbulence and chemistry. However, their dependence on numerous sub-models, the need for case-specific calibration, and their high computational costs limit their practicality for extensive parametric studies and control development. SRMs and CFD-coupled approaches reduce computational expense to some extent, yet they remain sensitive to tuning parameters and often retain an implicit dependence on CFD data. The multi-zone model (MZM) is a computational approach used in closed-cycle simulations to divide the combustion chamber into multiple control volumes or zones. An MZMs advantages include its capacity to represent spatial variations in the temperature and species concentrations inside the combustion chamber, improving predictions of engine performance and emissions [20]. Physics-based MZMs, extensively reviewed by Vasudev et al. [20], have emerged as a compelling intermediate framework, capable of capturing essential thermal and compositional stratification effects while achieving orders-of-magnitude reductions in simulation time. This method balances the required level of detail with the computational efficiency needed for practical engine development [21]. However, many existing MZMs rely on CFD-derived initialisation, ad-hoc calibration of zone evolution, or limited portability across engine platforms and operating regimes.

Since the first implementations of MZM for RCCI engines, the accurate representation and tunability of HRF stratification have been significant challenges. Egüz et al. [22] used an MZM combined with detailed kinetics to explore the auto-ignition behaviour of a dual-fuel RCCI engine. The authors used a 10-zone model to initialise the fuel distribution of diesel (represented by n-heptane) and gasoline (represented by iso-octane), based on 3D simulations and applying the interzonal mixing intensity as a tuning factor. They concluded that this mixing factor plays a crucial role in predicting emissions and performance, advocating a more efficient approach than CFD for modelling fuel distribution. Eichmeier et al. [23] presented a spray-based MZM, with a zonal configuration adaptively shaped through the spray development. They used Hiroyasu's packet [24] approach to develop a fast model to predict the pressure curve of a gasoline-diesel RCCI engine. A CFD-calibrated model estimated the turbulence length scale and turbulence dissipation. Although methodologically significant, their predicted combustion regime suggested separate HRF and LRF consumption, which is inconsistent with the experimental results. Mikulski et al. [25] introduced zonal lambda distributions across onion-skin configurations, where HRF concentration increases toward the outer zones. They employed tunable parameters to calibrate the fuel distribution, achieving predictive accuracy for combustion indicators, such as CA50 and IMEP, within the experimental cycle-to-cycle variation. The same model was employed to study the effect of LRF stratification within the cylinder, imposed by direct gas injection [26].

The fidelity and accuracy of all RCCI simulation tools (including the MZM) are directly related to the chemical kinetic mechanisms (CKMs) [27]. Recent MZM implementations have suggested a novel approach to address the complexity and fidelity of CKMs. De Bellis et al. [28] developed an MZM architecture to simulate a marine dual-fuel engine in RCCI. Instead of solving the chemistry in the simulation loop, they employed an ignition delay matrix, using a calculation based on a reduced-order CKM, to predict the onset of ignition in unburned zones. Instead of employing interzonal mass transfer, they considered a CFD-tuned simplified submodel to capture the effect of flame propagation, and incorporated an independent submodel to predict the emissions. They concluded that flame propagation plays a significant role in high-load operations, similar to the conventional dual-fuel mode. They considered a tuning parameter for the HRF, which was replaced by an empirical relation in their later study [7], where a comprehensive MZM (including interzonal mass diffusion) was introduced and validated for a single-cylinder engine using six explicit tuning constants. This approach also allows integration with commercial engine simulation tools, like GT-Suite.

The UVATZ (University of Vaasa Advanced Thermo-Kinetic Multi-Zone) model is a chemical kinetics-based multi-zone combustion model originally designed to simulate natural gas and diesel dual-fuel RCCI combustion. It discretises the cylinder into 12 chemical reactors, including disc-shaped zones representing the cylinder head and piston boundary layers, and annular zones which capture bulk inhomogeneity. The heat loss to the cylinder walls and interzonal heat and mass flows are modelled using gradient-based transport equations [29]. Kakoee et al. [30] coupled the UVATZ closed-cycle solver to GT-suite commercial software, proposing the resultant GT-UVATZ as a comprehensive RCCI simulation toolchain. This configuration of UVATZ demonstrated accurate predictions across six experimental cases ranging from 11% to 83% engine load. This was achieved through case-specific tuning of the fuel distribution and in-cylinder initial temperature. However, combustion prediction still relied on three calibration parameters, two of which had to be adjusted for each operating point. This setup provided good agreement with the experimental data for the Wärtsilä W31 engine, but its dependency on manual, case-by-case calibration limited its broader applicability. Mikulski et al. [31] presented the evolution trend of UVATZ, particularly by incorporating a CFD-validated turbulence model and integrating it with open-cycle solvers. These advancements

have applications in various fields, including exhaust aftertreatment and engine control. Salahi et al. [32] effectively reduced the UVATZ modeĺs runtime by decoupling chemistry equations from the heat and mass transfer calculations.

There is a knowledge gap in estimating the HRF distribution in RCCI due to the early injection and fundamental differences in the spray role between RCCI and diesel engines. Nazemi et al. [33] studied the effect of four injection parameters (spray angle, injection timing, premixed ratio and rail pressure) on light-duty RCCI combustion using CFD analysis by Converge integrated with GT-Suite software. They showed that the spray characteristics have a major effect on optimising RCCI performance and emissions. Kakoee et al. [34] investigated the effect of the start of injection (SOI) on HRF distribution in large-bore engines. Based on the results of their CFD study, Vasudev et al. [5] advanced the autonomy of the UVATZ by proposing a CFD-tuned turbulence model. The HRF concentration was assumed to depend only on the SOI, total HRF mass and inlet density. Thus, a two-level, full-factorial CFD study was designed to create a linear model for predicting the HRF equivalence ratio of the last zone. This correlation, along with the advanced turbulence model, showed acceptable results versus experimental data from the Wärtsilä W6L20 engine. However, this approach was tied to a specific zonal configuration and qualitatively adjusted to reproduce the experimental heat release rate (HRR) profile. It allowed broad freedom in tuning the HRR shape, but the method lacked a systematic basis and could not be generalised across different engines.

Building on these findings, a central limitation in current RCCI multi-zone modelling becomes evident. While MZMs are established as reliable system-level simulation tools, their robustness remains dependent on effort-heavy, CFD-informed stratification inputs and lumped chemical kinetic mechanisms. This reduces predictivity, implying case-dependent tuning and thus limits model transferability across platforms and fuels.

The present work aims to overcome this limitation by addressing the fundamental weaknesses of the University of Vaasa's advanced thermokinetic multi-zone model (UVATZ). First, the approach integrates systematic reactivity scaling to address chemical-kinetic deficiencies that were previously addressed by initial temperature adjustment. This methodology is investigated across two different chemical mechanisms by Yao et al. [35] and Salahi et al. [36]. Then, a generalised beta-distribution-based stratification model, which removes reliance on CFD-derived mixture profiles. It also provides a basis for automatically discretising the cylinder volume, which previously required manual adjustment to tune the HRR shape. The physical consistency is verified against detailed CFD spray simulation results.

The framework is encapsulated in a modular solver architecture and a structured calibration methodology requiring only limited test bench data to achieve full predictive capability. This is experimentally verified by testing the model performance against 40 RCCI operating points measured on a prototype Wärtsilä W31 medium-speed dual-fuel engine.

2. Methodology

2.1. The UVATZ framework

This study builds upon earlier versions of the University of Vaasa Advanced Thermokinetic Zonal model (UVATZ), a rapid and predictive simulation tool for RCCI combustion. Table 1 summarises the modeĺs key development stages. Notably, what is referred to as development version 2.0, introduced by Kakoee et al. [30], is functionally based on UVATZ 1.0, which was originally proposed by Vasudev et al. [29] in 2022. Version 2.0́s contribution is its full-cycle integration with GT-Suite, enabling dynamic coupling of closed-cycle combustion with open-cycle gas exchange. Introduced in 2024, UVATZ 3.0 aimed to reduce the case dependency of the calibration process through a fundamental flow study. In this version, a comprehensive turbulence model was proposed and calibrated from the CFD results.

UVATZ 4.0, developed in the present study, integrates all available submodels into a new modular object-oriented architecture, as illustrated in Fig. 1. Unlike the previous versions, both the Cantera-native, modified and UVATZ-specific submodels are treated as subclasses and are called sequentially at each solver step. This design provides essential flexibility for deploying various chemical kinetic mechanisms (CKMs) within an adaptive zonal configuration. It also facilitates inclusion of additional phenomenological submodels and solvers, without requiring the restructuring of the governing equations.

The Cantera CVODES solver [42] was used to govern the closed-cycle simulation. The fuel injector and intake/exhaust valves were modelled using flow devices connected to the reactor network. All these objects are native to Cantera 3.1, an open-source chemical kinetic suite: the original reference [38] describes their functionality. The Cantera wall object was modified to calculate the overall heat transfer based on the wall and bulk temperature differences, rather than the boundary zone temperatures in the standard implementation. This provides consistency with the heat transfer model calibration. Correspondingly, interzonal (cross-reactor) heat and mass transfers were implemented based on the Cantera wall and mass flow controller objects. A separate wall was considered for each reactor to impose an artificial heat transfer equivalent to fuel evaporation. Evaporative cooling was applied to the individual zones, following the external fuel-distribution submodel described in detail in Section 2.1.2.

The well-established Woschni-Chang heat transfer model [39], inherited from UVATZ 2.0, was extended for this study with a finite element method (FEM)-based wall thermal solver to update the cylinder wall temperatures on each cycle. Given the high thermal sensitivity of

Table 1
Evolutionary trend of UVATZ state of the art [31].

	UVATZ 2.0/GT-UVATZ	UVATZ 3.0	UVATZ 4.0
Platform	C++ source codeCantera 2.5 0D libraries [37] GT-Power user code	UVATZ 2.0+ GT-Power combustion object	Cantera 3.1 0D libraries [38]
Thermal and fuel stratification	12 zones (10 cylindrical + 2 disc-shaped) Spatial-dependent heat and mass transferImposed fuel distribution	12 zones (10 cylindrical + 2 disc-shaped)+ CFD-calibrated fuel distribution model	Flexible number of zonesGeometric fuel distributionAdaptive resolution
Submodels	Wall heat loss: Chang et al. [39]CKM.: Yao et al. [35]turbulence: Yang and Martin [40]	+Turbulence: Energy cascade [41]CKM: Yao et al. [35] + NOx	+Accelerated solver [32]Multi-chemistry+Wall temperature FEM solver [17]
Advantages over earlier	Integration with GT-PowerFull-cycle analysis	Emission calibrationMulti-cylinder simulationIntegration with optimiser	Object-oriented multi-role architectureValidated against 40 experimental data points
Tuning parameters	Zonal resolution: globalTurbulence intensity: globalFuel distribution: 2x localInitial temperature: local	Zonal resolution: globalWall temperatures: correlatedFuel distribution: correlatedTurbulence: engine-dependentManifold temp.: global	Reactivity multiplier: correlatedTurbulence intensity: globalFuel distribution: metamodel
Validated on	Wärtsilä 31 SCRE/RCCI (6 cases)	Wärtsilä 6L20/RCCI (3 cases)	Wärtsilä 31 SCRE/RCCI (40 cases)
References	Kakoee et al. (2023) [30]	Vasudev et al. (2024) [5]	Current study

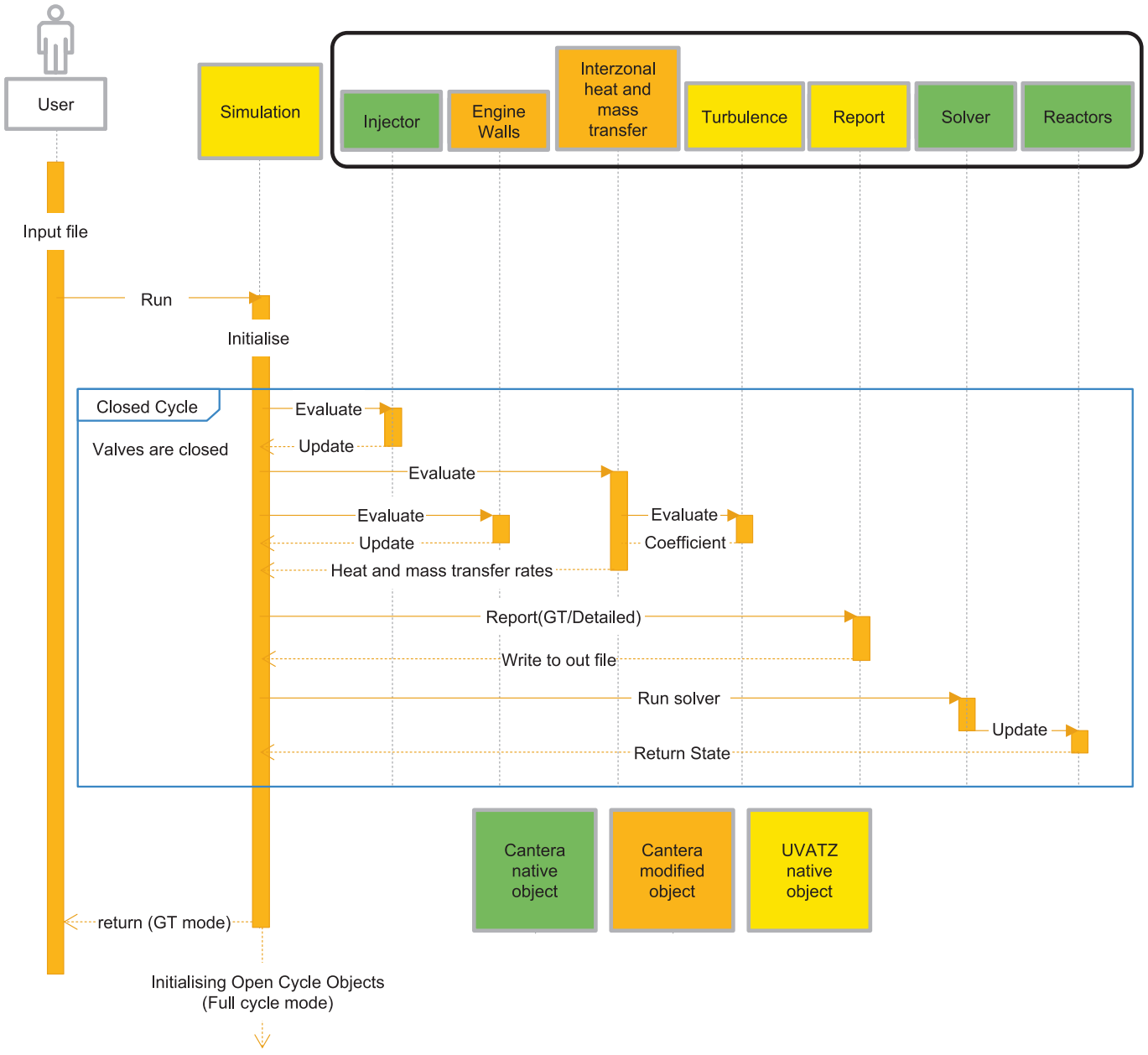

Fig. 1. The architecture of UVATZ 4.0 closed-cycle simulation.

RCCI combustion, this improved solution exhibits better predictability and autonomy than the fixed wall temperature approach used in earlier versions [17]. The phenomenological upgrades also included a new fuel-flexible chemical kinetic mechanism developed by Salahi et al. [36]. It comprises 60 species and 372 reactions, including methane and ethane as natural gas species and n-heptane as the high-reactivity fuel. Together with the well-validated turbulence model by Yang and Martin [40], this provided a CFD-independent simulation toolchain. The following subsections describe the zonal setup and submodels relevant to the studýs objectives.

UVATZ 4.0 was implemented in GT-Suite using an external cylinder object [43]. This approach offers greater control over the simulation and produces more accurate pressure and temperature readings than the combustion object, which only calculates the burn rate. As illustrated in Fig. 1, the simulation object is initialised according to the input file and chemical kinetic mechanism. Three external walls representing the piston, liner and head connect the boundary zones to their corresponding ambient temperatures, which are defined in the input file. Interzonal heat and mass transfer were implemented using Cantera wall and mass flow controller objects. All coefficients were updated at each step, based on the corresponding turbulence model and thermodynamic properties of each zone. At the end of each timestep, the reactor network is solved, and the results stored and delivered to the open-cycle solver.

2.1.1. *Chemical reaction rates and reactivity multiplier*

The reaction rates are calculated using the information embedded in the CKM file. For any elementary reaction declared in the CKM, the reaction coefficient k_f calculation is based on the modified Arrhenius relation, where the coefficients A, b, and E_a are reaction-specific constants defined in the CKM file.

$$k_f = AT^b e^{-\frac{E_a}{RT}}, k_f^{MZM} = M \times k_f \quad (1)$$

This study introduces a reactivity multiplier (M), which is applied equally to all individual reaction rate coefficients in the chemical source term. It controls the in-cylinder reactivity without altering the thermo-

dynamic boundary conditions. This approach addresses the limitations of previous UVATZ implementations, which were tuned by adjusting the initial cylinder temperature or, in some cases, the manifold pressure and temperature [5,30]. These temperature corrections successfully advanced the combustion timing, but compromised the simulation consistency with the 1D-solution by overriding the airpath calculations and wall heat transfer dynamics.

Applying a single reactivity multiplier to all forward reaction rate constants should be understood as a global time-scale adjustment rather than a physically rigorous modification of individual chemical kinetics. By uniformly scaling the forward rates, the relative ordering of reaction pathways, chain-branching structure, and competition among reactions is preserved, such that the qualitative combustion mechanism remains unchanged. In this sense, the multiplier retains the topology of the chemical network while accelerating or decelerating its overall evolution.

At the same time, this treatment sacrifices chemical fidelity at the level of individual reactions and species. Reaction-specific temperature sensitivities, pressure dependencies, and differential uncertainties in elementary rate constants are not represented. Consequently, the approach is not intended to improve species prediction accuracy or replace detailed mechanism refinement, but rather to provide a pragmatic correction for global combustion timing (e.g., ignition delay or heat-release phasing) where computational efficiency and robustness are prioritised.

The need for correction stems from the fact that reduced-order CKMs are developed using constant-volume reactor data and do not fully capture the complex turbulent mixing present in real engines. The M-multiplier provides a localised and physics-consistent method for reactivity calibration, enhancing model adaptability without disrupting coupled submodels. Consequently, the multiplier is considered a key tuning parameter during model calibration, described in Section 2.2.

2.1.2. Basic assumptions for the injection and resulting fuel distribution model

This study develops a scalable and geometry-independent solution by applying a geometrical function which distributes the injected fuel mass based on the non-dimensional volume of the cylinder $\overline{V}$ (ranging from 0 at the cylinder axis to 1 at the liner position). This function enables a physically meaningful, scalable and tunable fuel distribution across the zones. Accordingly, the non-dimensional volumetric fuel concentration (f) is defined by Eq. (2) as the local density of the HRF at each radial location of the cylinder.

$$f = \frac{1}{m_{inj}} \frac{dm}{d\overline{V}} \tag{2}$$

Fig. 2 illustrates an exemplary mapping of the cumulative fuel distribution derived from a real spray projection image. The grayscale background corresponds to the spatial distribution of projected fuel intensity, whereas the superimposed curve represents the cumulative integration of fuel mass along the spray axis. The monotonic yet nonlinear shape of the cumulative curve indicates that a larger portion of the injected fuel mass accumulates within specific regions, reflecting the combined effects of spray breakup, evaporation, and entrainment processes. Based on this, the fuel density function can be assumed to be a nonlinear function with the following governing assumptions: (i) mathematically, f must be a probability density function normalised to the mass of the fuel injected per cycle (m_{inj}). (ii) physically, the average mass of the spray on every local $d\overline{V}$ is sensitive to at least one distributive point (initial injection point, $\overline{V} = a$) and one resisting point (terminal point colliding with the ambient/wall, $\overline{V} = b$).

Considering the governing assumptions i and ii, f can be expressed via Eq. (3):

$$f(\overline{V}) \propto (\overline{V} - a)^{r_1} (b - \overline{V})^{r_2} \tag{3}$$

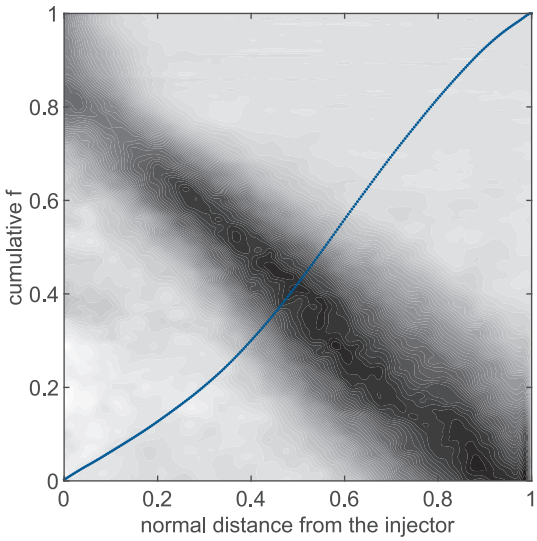

Fig. 2. Fuel distribution in a real spray image (adapted from Sandia spray M database [44]).

Equation (3) suggests a functional form of the beta distribution density function [45], and its exponents r_1, r_2 represent the model's sensitivity to the initial injection point a, and the terminal resistant point b, respectively. The injector is at the centre of the cylinder, so a can be assumed to be 0. In addition, in RCCI early injection cases, the evaporated spray hits the wall before combustion begins [34]. Therefore, b = 1, and the function can be written in the standard form (Eq. (4) where the exponents are α -1 and β-1.

$$f(\overline{V}, \alpha, \beta) = \frac{\overline{V}^{\alpha-1}(1-\overline{V})^{\beta-1}}{B(\alpha,\beta)} \tag{4}$$

The parameters α and β define the function shape by determining the slope (fuel concentration growth) at the beginning and end of the spray, respectively. Namely, the $\alpha = \beta = 1$ yields a uniform fuel distribution, and decreasing β (while increasing α) shifts the fuel concentration towards the cylinder wall. The evaluation of these parameters is described in Section 2.2 (model calibration).

2.1.3. Zonal configuration, in-cylinder mixing and combustion evolution

The zonal configuration followed the approach of Vasudev et al. [29], where two disc-shaped, non-reactive zones connected to the walls were

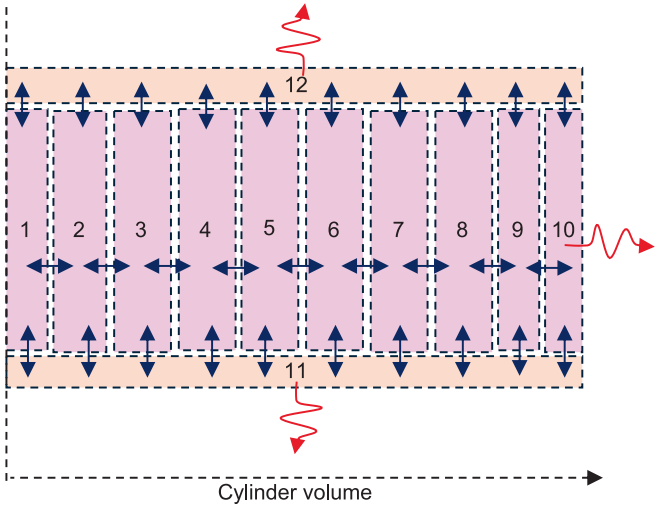

Fig. 3. Zonal configuration of the UVATZ closed-cycle model.

introduced to better capture the effect of unburnt hydrocarbons (Fig. 3). However, the current study adapted the approach to discretise the cylinder volume. The volume fraction of zones 6–10 was calculated to contain an equal amount of HRF, based on the cumulative beta function described in Section 2.12. Zones 1–5 were assumed to have similar volumes to zones 10–6 in a symmetric manner. This symmetry promotes rapid combustion propagation in the highly reactive wall-adjacent zones while delaying ignition penetration toward the cylinder centre, contributing to a smoother heat-release rate (HRR) profile.

The upper and lower zones are initialised with 10% of the cylinder volume (5% each). This value is subject to change due to moving boundaries and internal mass diffusion derived according to Fick's law. Eq. (5) describes the mass transfer from zone i to adjacent zone j as follows:

$$\dot{m}_{i\to j} = Ct\left(\frac{D_w A}{\delta}\right)_{ij}\rho_i, Ct = 0.41 r_n^+\left[1 - exp\left(-0.0492 r_n^+\right)\right] \quad 5$$

where A is the contact area, and δ is the distance between the zoneś centres. The diffusion factor (D_w) calculation is based on the unity Lewis number; and the turbulence intensity (Ct) is determined by the Yang and Martin [40] approach, based on non-dimensional distance from the liner (r_n^+). Readers are encouraged to refer to Vasudev et al. [29] for more details.

The interzonal mass transfer was enabled only after 1% of the total fuel mass was consumed. This ensured that the species distribution remained according to the adopted spray model at the ignition onset (refer to Section 2.1.1). It reduced the computational cost by avoiding redundant species transport calculations during the premixed phase.

Note that combustion propagation is captured in MZMs by interzonal mass and work transfer [19]. As illustrated in Fig. 4, combustion initiates in the highly reactive zones, which expand and compress the adjacent zones, thereby promoting their ignition. The expansion of the burning zone also causes a sharp drop in the local density, resulting in net mass transfer from the inner to outer zones (Eq. (1), which facilitates the growth of the burned region.

2.1.4. The 1-dimensional engine model and model-coupling methodology

The present work inherited the airpath model from UVATZ (2.0). A 1D model of the reference single-cylinder research engine (Wärtsilä Mono) was developed using GT-Suite simulation software. The model provides a detailed discretisation of the airpath and, following the SCRÉs standard four-valve layout, includes a comprehensive charge air system and the complete exhaust stack. The exhaust section included the actual pipe geometries of the test cell, buffer tank and regulated back-pressure valve. The discretisation lengths for all flow components were 124 mm for the intake and 170 mm for the exhaust. The reader is referred to the original work by Kakoee et al. [30] for further details of the airpath model.

This study adopted the coupling methodology conceptualised by Kakoee et al. [30] for UVATZ 2.0. However, version 4.0 implemented several technical enhancements to ensure that the model remains robust across a wide range of operating conditions and input parameters. First, the file-handling routines were improved to support reliable communication between the user code and the multi-zone model. A fixed file path is now assigned for the UVATZ executive and CKM file, while input/output files are detected dynamically, as the MZM is always invoked from within the GT model file directory. This dynamic handling is essential for enabling compatibility with the GT-Power parallel solver and integrated optimiser.

There are inconsistencies between GT-Suite and chemical kinetic mechanisms in terms of species names, so the model was updated to explicitly pass fuel species names to UVATZ. Burned species, which GT-Suite tracks by default for exhaust flow calculations and residual estimation, are predefined internally. Standardising communication based on species names means the model remains compatible with a wide range of CKMs. This approach also improves the simulation efficiency, as only the key species required for engine modelling are reported to the user code, avoiding unnecessary crank angle-resolved tracking of intermediate species, which is especially valuable when working with large kinetic mechanisms. However, this compact reporting scheme applies only to open-cycle simulations. Closed-cycle simulation always utilises the full CKM to capture the detailed combustion chemistry. Fig. 5 shows the major data flow structures between the commercial GT-Suite solver and the UVATZ executable.

2.2. Model calibration and validation

The model was validated using a two-stage procedure. First, the beta-function-based fuel distribution model (introduced in Section 2.1.3) was assessed for its ability to reproduce the fuel stratification effects observed in real engine operation. This validation was performed using data from the Wärtsilä 6L20 engine, derived from both spray chamber experiments and RCCI-mode CFD simulations. These datasets provide a reliable reference for evaluating the phenomenological accuracy of the proposed stratification model.

After confirming its physical validity, the second stage involved a full model calibration for the Wartsila 31 engine geometry. This stage relied

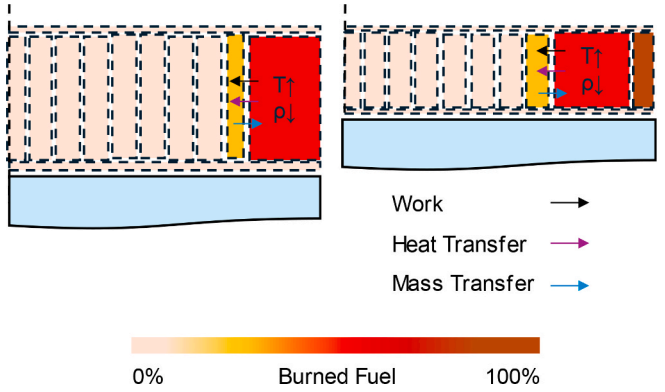

Fig. 4. Two frames of the UVATZ simulation showing combustion propagation performance.

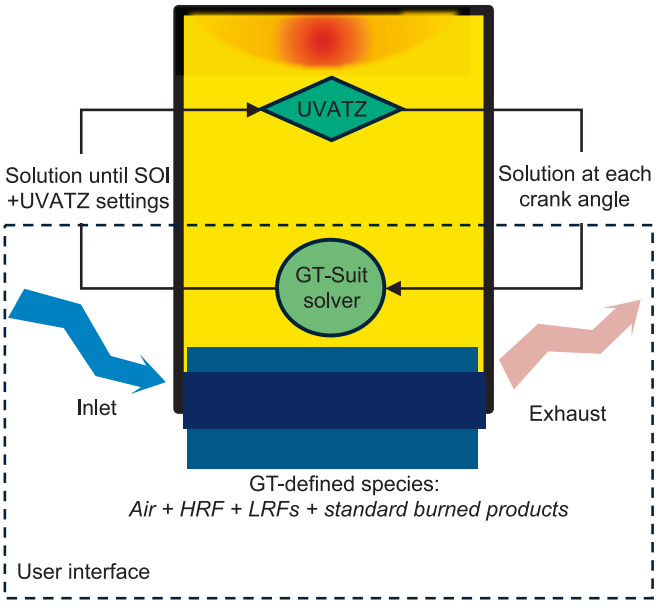

Fig. 5. Architecture of UVATZ 4.0 coupled with GT-Suite showing the flow of data between both solvers.

exclusively on engine testbed data, without any CFD-derived spray or combustion profiles. This approach aligns with UVATZ 4.0s core objective to provide a scalable and predictive RCCI simulation framework, fully independent of high-fidelity CFD inputs.

2.2.1. Phenomenological validation of the fuel distribution model, based on CFD data

CFD results from [34] were used to validate the HRF distribution function. That study was initially undertaken to examine the effect of the SOI on HRF distribution. The validation process involved comparing the CFD models in-cylinder pressure curve and HRR profile with experimental data from the Wärtsilä 6L20 dual-fuel engine operating at 50% load. The simulation was conducted in reactive mode in a closed-loop model without considering the ports and valves directly in the simulation. The head, piston and liner temperatures were set to the measured data. The initial values for the pressure and temperature were assumed to be the intake and exhaust port conditions. A nonreactive CFD simulation, including in-cylinder valve motion, was conducted to provide intake valve closing (IVC) conditions for the reactive simulation. Accuracy and reliability of the CFD model were assessed using a mesh sensitivity analysis. Once validated for one point, a sweep analysis of the SOI was performed to investigate the spray phenomenon. Table 2 gives more details and the selected SOIs for this study. Readers are encouraged to refer to the original study [34] for further information.

2.2.2. Calibration of the UVATZ framework based on the test-bed data

To achieve a physics-based generalisation of the MZM, three concrete steps were designed to ensure the scalability and robustness of the solver over a wide range of input conditions. As shown in Fig. 6, the prerequisite for starting the UVATZ calibration is calibration of the airpath model. This usually is performed for selected (three to 10) operating points via so-called three-pressure analysis (TPA) to ensure correct IVC conditions in the cylinder. The procedure is standard for all GT-Suite engine models and will not be discussed here: the reader is referred to the GT user manual [43].

After flow calibration, the combustion calibration proceeded with all operating points used to evaluate the reactivity multiplier (M in Eq. (1). The calibration problem illustrated in Fig. 7 can be reduced to a two-variable optimisation procedure. The reactivity level is bounded within the low limit, below which all HRF distributions lead to misfire, and a high limit above which the mixture will auto-ignite too early. Between these two extreme limits, there should be a space of feasible answers. To isolate the effect of the HRF distribution, a range of probability density functions (Eq. (4) was assessed, spanning from a uniform fuel distribution ($\alpha = \beta = 1$) to a highly concentrated one ($\alpha = 2$, $\beta = 0.2$). The objective was to minimise the difference between the simulated and measured values of IMEP and peak in-cylinder pressure (Pmax), with a tolerance limit of 5%. Analysing the sensitivity of case-dependent tuning across various operating conditions enabled the proposal of a mathematical model to predict reactivity, based on the most effective operating variable(s).

Following reactivity calibration, the next step was tuning the fuel distribution. As mentioned in the previous section, varying the β (Eq. (7)

Table 2
Reference CFD study [34] to validate the HRF distribution function.

Displacement & nominal speed	8.8 l/1000 rpm
Stroke/bore	1.4:1
Turbulence model	Reynolds-averaged Navier–Stokes (RANS) - re-normalisation group (RNG) k-ε
Mesh generation	dynamic, unstructured grids
Wall heat transfer model	O'Rourke and Amsden
Breakup model	Rayleigh–Taylor
SOI (CAD bTDC)	66, 72, 78, 84
Injection duration (CAD)	2.5
Natural gas mass fraction	0.0181

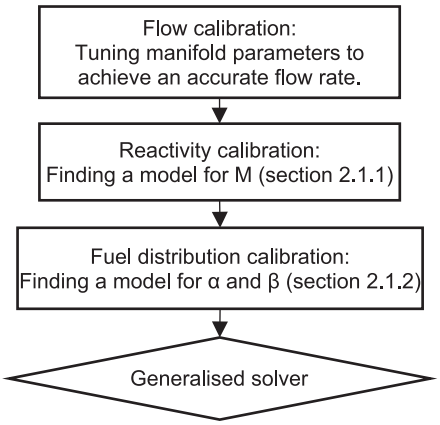

Fig. 6. UVATZ 4.0 calibration flow chart.

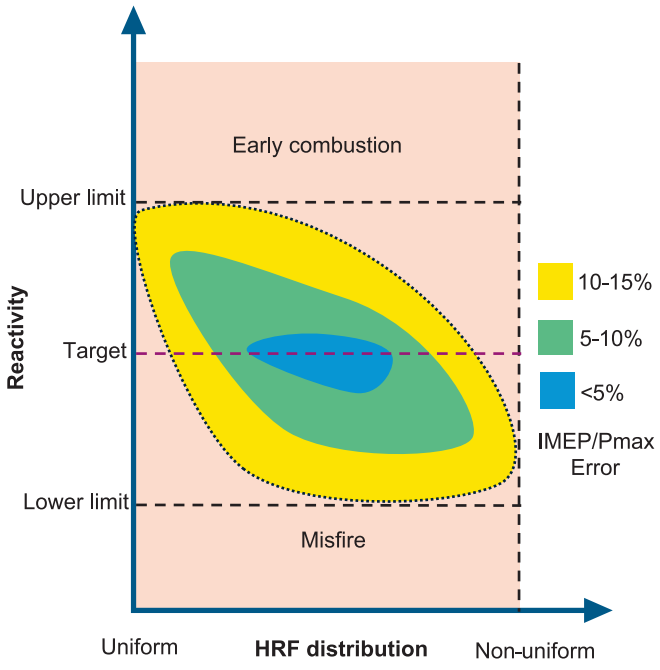

Fig. 7. Calibration process defined as a two-variable optimisation problem.

from zero to one yields a range of distributions from highly concentrated to more uniform. In this step, the objective was to minimise the RMS error of the entire simulated pressure trace, which automatically translates to an accurate reproduction of IMEP, Pmax and combustion indicators (CA10 - CA90). The improved file management system and parallel simulation capability of UVATZ 4.0 enabled the use of the GT integrated design optimiser to identify the optimal tuning parameters for each case.

2.2.3. Reference experimental data for calibration

The RCCI validation data in this study were obtained from the Wärtsilä Mono single-cylinder research engine (SCRE), which mimics the cylinder geometry of Wärtsilä's 310 mm-bore dual-fuel production engines. Table 3 lists the main characteristics of the Wärtsilä SCRE and the experimental setup.

A centrally positioned twin-needle injector within the high-pressure common rail fuel system was optimised for use with light fuel oil (LFO) as the HRF [46]. During dual-fuel operation, the smaller needle ensures the accurate delivery of small pilot fuel doses, whereas the larger needle is used only in diesel mode. A smaller nozzle improves the atomisation of

Table 3
Specification of Wärtsilä Mono single-cylinder research engine

Displacement & nominal speed	32.45 l/720 rpm
Stroke/bore	1.39:1
Air system	External air compressor with air temperature and pressure control (up to 10 bar)
High-reactivity fuel system	Common rail 2.0 with twin needle injector and multi-injection capability (2000 bar)
Low-reactivity fuel system	Low-pressure, multipoint, upstream of the intake valves
Valvetrain	Four valves with swirl + tumble ports; variable intake valve closure (IVC); fixed exhaust valve opening (EVO)
Emission system	Horiba Mexa-One (NOx, CO, THC, CO_2, O_2) AVL415S (FSN-soot)
Indicative system	AVL Indicom cylinder pressure transducer Kistler 6124A, 300 bar range, 30pC/bar sensitivity.
Engine control	Rapid prototyping platform
Test fuels	ISO 8217-compliant LFO and LNG

micro-injected quantities in RCCI injections. The narrow-cone injector tip further supports proper reactivity stratification, while avoiding wall wetting at early injection timings. Natural gas, the low-reactivity fuel (LRF), was supplied via a multipoint gas injector located upstream of the intake valve. The SCRE features partially variable intake valve actuation.

The measurement system included high-frequency acquisition (0.2 CAD resolution) of in-cylinder pressure and pressures in the individual valve ports upstream and downstream of the combustion chamber. Pressure signals were filtered, pegged [47], and averaged over 300 cycles. The maximum deviation from the individual cycles was used to determine the uncertainty of the recorded pressure traces in the context of model validation. Note that in RCCI, stochastic variations in combustion have a greater impact than cumulative errors from the pressure transducer and optical encoder (discretisation error) [48], and offer a more meaningful measure of uncertainty encompassing random boundary condition deviations. Post-processing of the in-cylinder pressure to the gross heat release rate (HRR) was performed using the second law of thermodynamics, assuming a case-specific ratio of specific heats and a Woschni heat loss mode [49]. Note that the post-processing methods were the same for the engine and simulation data, providing consistency. Combustion indicators were the gross cumulative heat release (CHR) and the crank angle at which X% of the maximum energy released (CAX).

The definitions of indicated mean effective pressure (IMEP) and efficiency used in this study are standard [47] and will not be elaborated further. Low-frequency measurements track the consumption of each fuel type, using a gravimetric fuel balance for liquids and a Coriolis flow meter for gases and air intake. Additionally, thermal characterisation data of the intake and exhaust ports, along with temperature measurements of the piston top, liner, valves and cylinder head surfaces were collected for model validation.

The scope of calibration, as illustrated in Fig. 8, encapsulated 40 RCCI operating points, representing both the engine load and individual control parameter sweeps. Light fuel oil (LFO) injection was initiated early in the compression phase in all instances, with the quantity precisely adjusted against the gas fuel value to ensure that combustion developed around top dead centre (TDC). Load adjustments were made by altering the total fuel value and the pressures at both the intake and exhaust pipe ends, effectively simulating a load sweep typical of a turbocharged multi-cylinder engine.

Further variations in the combustion control parameters were explored, particularly around the 50% load point. These included variations in the duration and timing of the LFO injection, as well as the intake air temperature. The injection timings and λ setpoints in Fig. 8 are shown as relative values with respect to the reference (production) engine calibration, due to confidentiality reasons. Finally, the sweeps involved varying the intake and exhaust valve closure (IVC/EVC) in a narrow range of 1.0 or 1.5 CAD.

3. Results

3.1. Fuel distribution model validation

Fig. 9 illustrates the CFD data used to validate the HRF distribution. Early injection cases were selected as they were more representative of RCCI conditions. The HRF fraction over the cylinder geometry at a crank angle of 16 CAD BTDC was assumed as the reference for this study, as it approximates the expected onset of combustion. In early injection cases, the vapour fuel fraction adhered well to the cylinder wall before ignition. This can be further observed for several explored SOIs in Fig. 10, where the cumulative HRF distribution is shown against the normalised cylinder volume. The phenomenology is consistent with the findings of several studies on spray distribution in early injection RCCI [33,50].

Eq. (4) suggests that two variables, α and β, can be used to determine the fuel distribution. To validate this assumption, a cumulative beta function was fitted to the CFD data points by minimising the R-squared error. Fig. 10 shows that the beta function can properly fit all CFD results (RMS error < 3 %). A constant alpha value can represent the initial

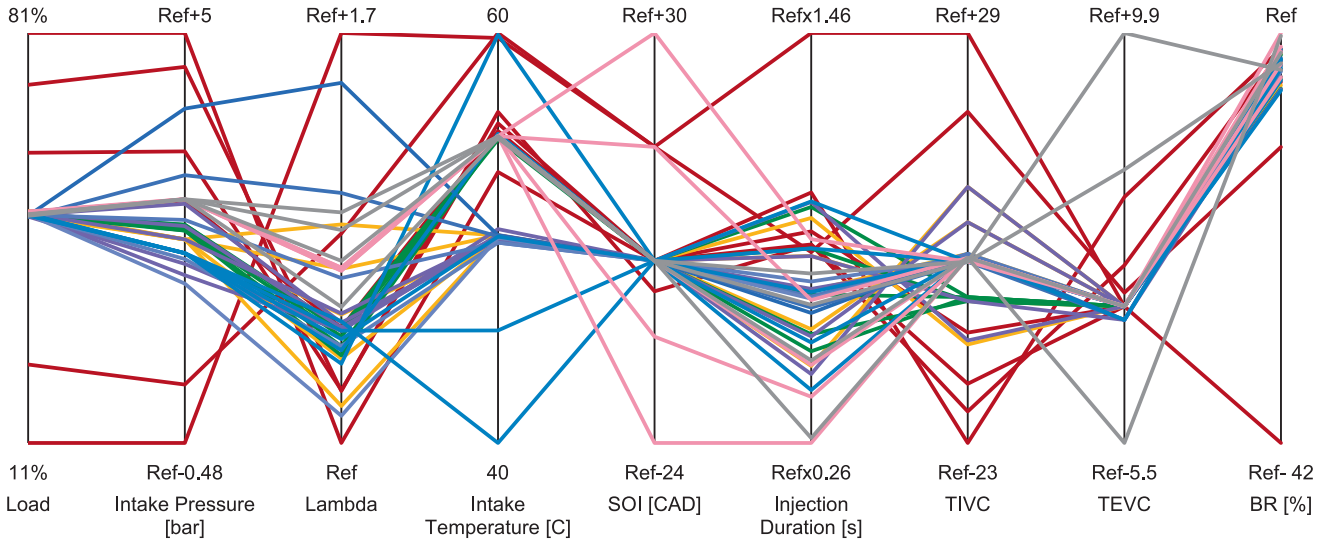

Fig. 8. 40 experimental RCCI cases (shown by lines), represented by the level of operating parameters: Ref denotes reference Wärtsilä 31DF calibration.

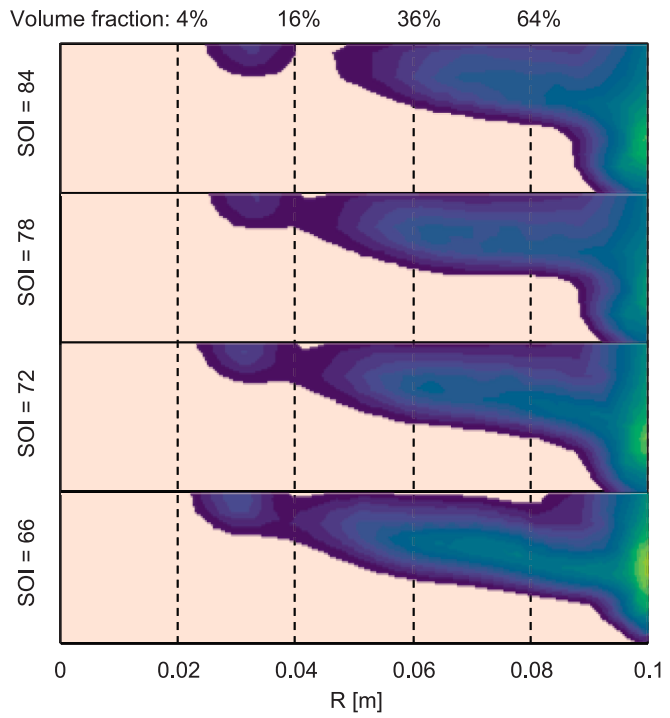

Fig. 9. Mass fraction of HRF at different SOIs at 16 CAD bTDC: the CFD simulation data for the Wärtsilä 6L20DF engine cylinder were adopted from Kakoee et al. [34].

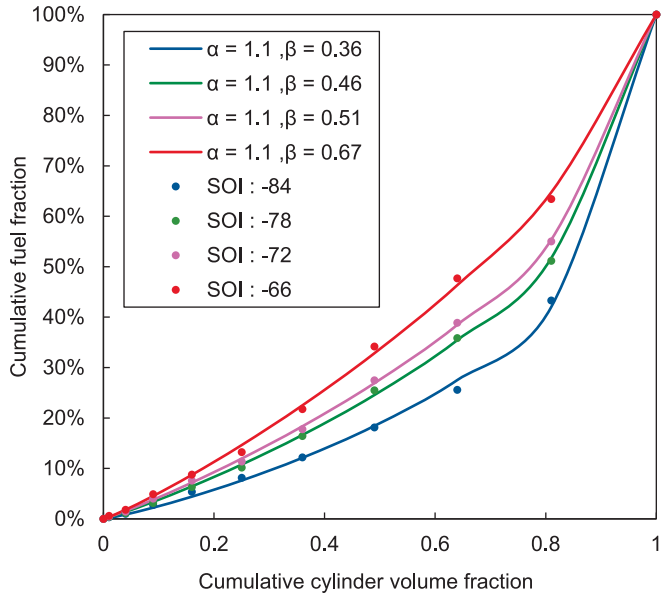

Fig. 10. Fitting the beta distribution function to the CFD data in Fig. 9.

behaviour of all HRF distributions, at least when the SOI sweep is considered. The β changes according to the foreseen phenomenology, with lower values representing fuel which is more concentrated around the cylinder liner. Note that such behaviour is characteristic of cylinder configurations with a weak tumble motion component. Pistons with distinctive bowl structures and high mean piston speeds sustain the intake-induced tumble, providing a more effective HRF redistribution along the cylinder axis [34]. In the studied configuration, the weak swirl flow dominates, which supports radial homogenisation, particularly with a multi-hole injector [51]. This is consistent with the governing assumption of onion skin MZMs.

3.2. Calibration based on mixture reactivity

Reactivity calibration was performed based on the strategy outlined in Section 2.2.2. The reactivity multiplier was case-dependently tuned to the experimental data and analysed for its dependency on engine operating variables. Table 4 shows that the strongest correlations with the reactivity multiplier were found in the boost pressure, low-reactivity fuel (LRF) mass and air mass. However, in RCCI operation, these variables are inherently interdependent. For example, an increase in fuel energy demand during a load sweep requires a proportional increase in the aspirated air mass to maintain ultra-lean combustion, which in turn necessitates an increase in the boost pressure. Given these dependencies and considering that LRF mass demonstrates both the strongest correlation and the most consistent linear sensitivity, LRF mass was identified as the governing variable influencing the reactivity multiplier.

Fig. 11 verifies the above assumption by comparing the two chemical kinetic mechanisms (CKMs) commonly used in RCCI combustion simulations. The Oulu60 mechanism, developed by Salahi et al. [36], was selected as the baseline for the current study, whereas earlier versions of the UVATZ model used the mechanism proposed by Yao et al. [35] .

It is evident that the Yao mechanism is significantly less reactive than Oulu60 and thus requires a higher reactivity multiplier to achieve stable combustion in the same engine setup. A key difference is their choice of HRF surrogate: Oulu60 uses n-heptane, whereas Yao et al. employ n-dodecane. Neither surrogate fully represents the multi-component LFO used as the HRF in an experimental engine. Oulu60 gave a closer match to the experimental results - often achieving a correlation coefficient near 1 - but it still oversimplifies the interaction dynamics between the HRF and LRF, especially under extreme LRF content (i.e., high or low LRF charge, at either end of the x-axis in Fig. 11).

An additional justification for applying a reactivity correction is the simplified representation of LRF in both mechanisms, which typically is limited to methane (CH_4) and ethane (C_2H_6). Actual natural gas compositions are more complex and are influenced by second-order species, as discussed in [52]. Furthermore, CKMs are often validated under limited conditions which do not fully align with the mixture strengths and thermodynamic environments encountered during real engine operations [53].

This analysis underscores the need to incorporate an LRF-dependent reactivity multiplier to compensate for kinetic mechanisms' limitations in reproducing realistic RCCI behaviour in multi-zone simulations. Consequently, an exponential correlation, as shown in Fig. 11 ($R = 0.45\exp(0.67m_{LRF})$) was adopted for Oulu60 and carried forward in the updated UVATZ 4.0 model.

3.3. Fuel distribution calibration based on engine experiments

Following the calibrated reactivity and the results in Section 3.2, the fuel distribution was optimised to achieve the best fit with the current engine platform. In this step, GT's integrated optimiser was used to minimise the RMS error of the pressure curve with respect to the experimental pressure data by adjusting only parameter β for each case. Three constraints were considered to maintain the maximum pressure, CA50 and IMEP close to the experimental values.

Fig. 12 shows how β can change the HRF distribution, and consequently the zonal configuration, as described in Section 2.1.1. Higher values form more uniform configurations, and lower values indicate a higher density near the walls, leaving a lower concentration in the inner zones.

Fig. 13 illustrates the optimisation results for two of the 40 cases studied. These cases were chosen to represent two distinct types of sensitivity to the HRF distribution. In certain instances, particularly when the optimal β is near unity (indicating a uniform condition), the trend of Pmax is monotonic and decreases as β increases. This is a natural behaviour because increased stratified reactivity can enhance combustion, thereby increasing the pressure rise. When the HRF is more

Table 4
Statistical analysis of reactivity multiplier concerning engine operating conditions.

	Blend ratio	LRF mass	Lambda	Diesel mass	Air mass	Boost pressure	SOI
Pearson coefficient	0.65	0.92	-0.54	-0.23	0.76	0.85	-0.47
Relative factor sensitivity(Linear R-Squared: 0.85)	-	0.74	-	-	0.14	0.12	-

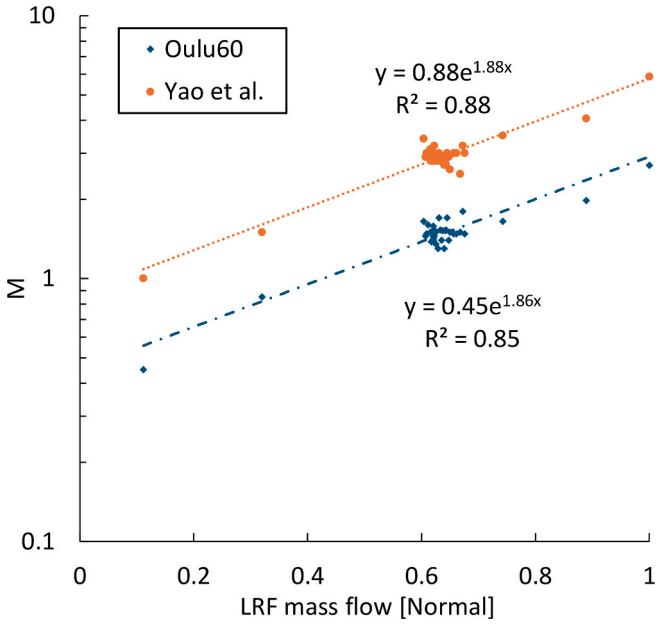

Fig. 11. Reactivity multiplier against LRF mass for Wärtsilä Mono operating points, simulated using two different mechanisms.

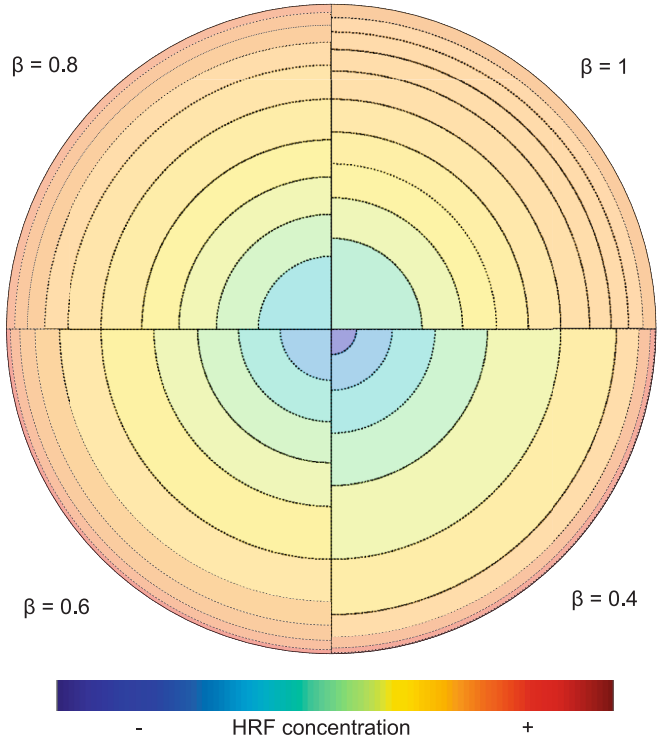

Fig. 12. Zonal configuration and HRF distribution related to different β values.

concentrated near the wall, Pmax initially increases and then decreases. This decline can be attributed to insufficient reactivity in the inner zones, which delays the propagation of combustion to those areas, even if it is initiated earlier in the outer zones. As is evident, the IMEP error is hardly affected by changing the combustion phasing by varying the fuel distribution, as long as the ultimate combustion efficiency is unaffected.

The objective was to find the global minimum of the RMS error of the pressure curve. As shown in Fig. 13, the global minimum can occur where local discontinuities are detected. Discontinuities are due mainly to the discretised domain, where the start of combustion can eventually shift from one zone to another. To obtain a robust solution, it is necessary to select the optimal point with a reasonable margin from the discontinuity, where a dense neighbourhood of legitimate results exists.

Similar to the reactivity multiplier, the impact of various variables on β was analysed. Among the various operational variables associated with each case, only timing of the intake valve closure (TIVC) and λ exhibited relatively strong correlations (-0.67 and -0.75, respectively) and linear R-squared values (0.45 and 0.57, respectively). Analysis of the trend of β over different sweeps (Fig. 14) indicated that TIVC has no independent effect on β when it varies with a fixed value of λ. In addition, λ was the key parameter determining β in all sweeps except the SOI sweep. Understandably, the SOI has a significant effect on the HRF distribution, as the early injection contributes to mixture homogeneity. However, the first six cases suggest that the blend ratio may reverse this effect. A lower blend ratio generally leads to a more concentrated HRF near the walls because a larger amount of liquid fuel sticks to the liner, which has a greater area at earlier injection times. This was confirmed by the experimental results of De Felice et al. [7] which indicated that injecting a high amount of HRF into a low-density chamber leads to a rapid penetration towards the chamber wall.

Therefore, a model based on the three variables (1/λ, SOI and BR) may suffice to approximate the HRF stratification. The selection of dimensionless variables contributes to a stronger generalisation and adaptability to any RCCI domain. To limit the range, the normalised SOI was defined as the dimensionless position of the piston with respect to the engine stroke at the injection time. A second-order polynomial was proposed to capture the effects of these variables. A sigmoid function was imposed on the polynomial output in order to avoid unrealistic, highly concentrated HRF which causes simulation instability.

$$\beta = \beta_{min} + (1-\beta_{min})\frac{1}{1+e^{-Q\left(\overline{SOI},\frac{1}{\lambda},BR\right)}} \quad 6$$

This notation guarantees that always $\beta_{min} < \beta < 1$. The polynomial contains the most effective quadratic terms and can be expanded as follows:

$$Q\left(\overline{SOI},\frac{1}{\lambda},BR\right) = \frac{A_1}{\lambda} + A_2\frac{\overline{SOI}}{\lambda} + A_3.\overline{SOI}^2 + A_4.\overline{SOI}.BR + A_5.BR + A_6 + A_7.\overline{SOI} \quad 7$$

These coefficients were calculated and are presented in Table 5, along with the corresponding p-values. β_{min} was considered to be 0.26. Fig. 15 shows the predicted values of β over their observed values. It also demonstrates how the sigmoid function prevents out-of-range values and enhances the extrapolation capability of the model. The complex impact of SOI is clear from its appearance in various terms with both negative and positive coefficients. SOI determines the combustion chamber density and can affect HRF distribution in two ways. A more advanced SOI implies a lower density in the combustion chamber, facilitating spray penetration and a more concentrated distribution.

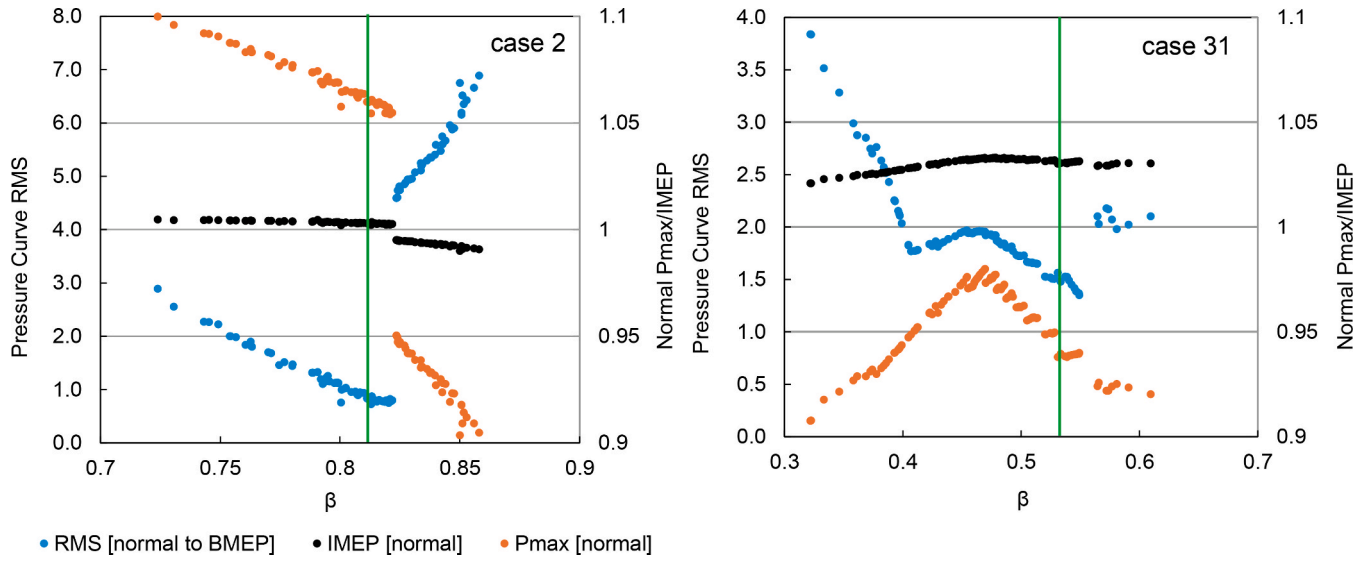

Fig. 13. UVATZ calibration results for exemplary operating points of Wartsila Mono RCCI campaign - Case 2 (72% load) and Case 31 (50% load).

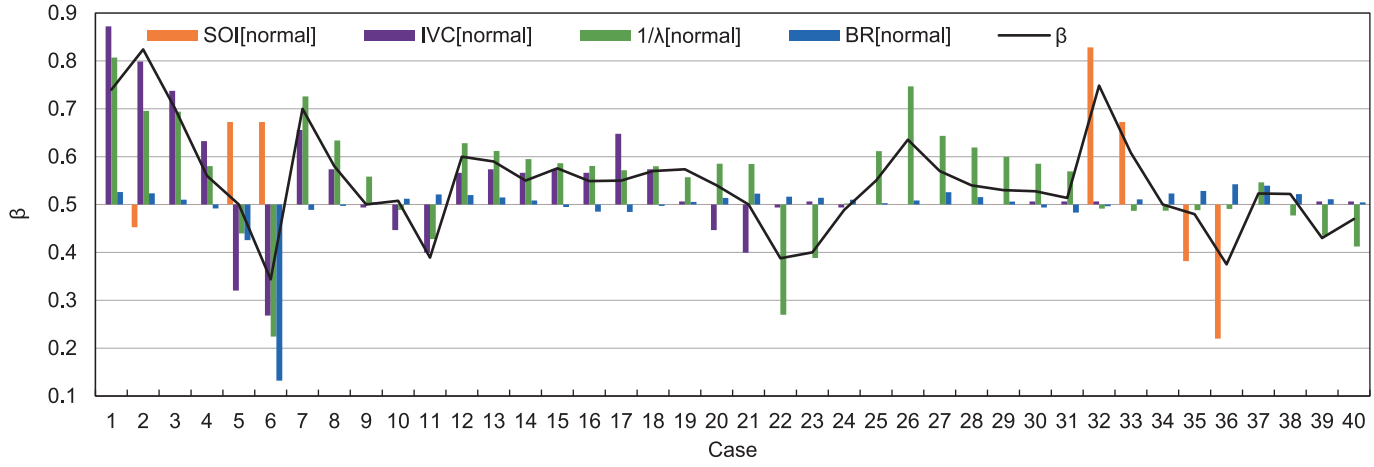

Fig. 14. Optimised values of β across different experimental cases.

Table 5
Fitted coefficients and p-values of Eq. (7).

Coefficient	A1	A2	A3	A4	A5	A6	A7
Value	392.02	741.85	22.36	-137.18	-69.98	-45.58	79.92
P_Value(95% confidence)	2.2E-07	5.5E-07	5.4E-05	8.6E-05	3.3E-04	2.4E-03	4.0E-03

Simultaneously, this means more resident time, leading to a more uniform distribution, owing to evaporation and mixing with the charge content. This dual effect is captured by the nonlinearities observed in the polynomial terms. This substantiates the importance of a predictive phenomenological HRF distribution model for advancing the state of the art in RCCI simulations.

3.4. Complete model validation

All 40 cases were simulated using the predicted values of β and M, and the quality of the results was evaluated against the experimental data. As illustrated in Fig. 16, the maximum pressure and IMEP for 80% of the cases were predicted with an error margin of within 5%. In addition, CA50 was predicted with a maximum error of 5 CAD and a standard deviation of 1.0 CAD. This highlights the model's reliability, without applying any case-by-case tuning. The first six cases suggested a descending trend in the CA50 prediction. The model tended to underpredict cases with low blend ratios. This can be justified by the fundamental assumption that the HRF is injected as vapour at the moment of injection. This assumption deviates from reality, especially in the case of high BR, low lambda with early injection (case 6 in Fig. 14). In such a case, the combustion performance tends to be in diesel mode, where the evaporation phenomenon is relevant.

Fig. 17 shows the pressure curves for the two cases with the greatest and smallest errors in the maximum pressure values. In both cases, combustion began rapidly, and the pressure surpassed the measured value at that moment. Fuel distribution was more uniform in case 13 (Fig. 14), so the size of the combusting zone was larger owing to the discretisation methodology, leading to a more significant increase in pressure. In this case, combustion propagates more easily to other zones because the zonal reactivity gradient is lower. In the other case (case 39), this occurred differently, resulting in a smoother pressure increase.

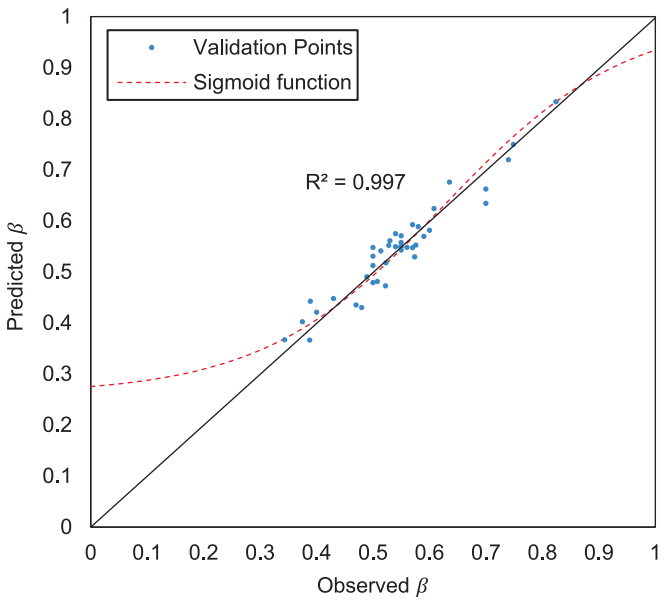

Fig. 15. Predictivity of β value among experimental cases

The staggered pattern of the cumulative heat release rate (CHR) charts clearly indicates that combustion phasing is influenced primarily by fuel stratification, as interzonal heat and mass transfer are much slower than chemical reactions. Heat release rate (HRR) charts clearly show that the last four or five zones close to the liner started combusting one by one, and the rest of the zones combusted simultaneously. Fig. 17 highlights the statistical relevance of the results compared with the uncertainty in the measured pressure data. The pressure was consistently predicted within the highest and lowest recorded values.

The overprediction of Pmax in case 13 is also associated with the phenomenon visible in the cases with more uniform HRF (like case 2 in Fig. 13). In these cases, both the first and last zones are larger and contain more energy value. It imposes a binary behaviour between two levels of overprediction and underprediction as discussed in Section 3.3. The HRR curve in these cases approaches that of a single-zone reactor, which accounts for the deviation from the experimental curves.

The non-smooth behaviour of the heat release rate at the onset of combustion is directly related to the limited number of zones treated as homogeneous reactors. In reality, the flames driven by the spray originate from a two-phase mixture of HRF particles and premixed charge, featuring a high vapour concentration gradient surrounding the droplets. This complicated phenomenon can hardly be captured with simplified 1D assumptions. However, engine performance indices such as IMEP, CA50, and CO_2 emissions were predicted well, regardless of the curve mismatch. This shows that the current model, as a system-level simulation tool, is suitable for control-oriented and optimisation studies over a broad range of operating conditions.

4. Discussion

The current studýs main contribution with respect to the previous UVATZ 2.0 work [30] is the proof of scalability and, more importantly, the removal of case-specific tuning parameters. In order to benchmark the current framework against the literature, the work by De Felice et al. [7] at The University of Naples was selected as another significant study in this sphere. That model was based on tabulated chemistry to predict the auto-ignition behaviour of dual fuel combustion. Unlike the UVATZ model, where chemical reactions and physical interactions drive all simulation outcomes, their model used separate submodels to enhance its capabilities, particularly to predict NOx and flame propagation. They considered some spray-affected zones based on the experimental shape of the spray to impose a reactivity gradient in the combustion chamber. Mass transfer was implemented in two distinct ways to capture both spray development and mass diffusion. Collectively, they introduced six tuning constants for all these submodels. The key advantage of this approach is its modularity, integrating well with GT-Suite. The use of tabulated chemistry enables finer discretisation, while maintaining appropriate fidelity. A simulation time of less than 2 min per cycle was reported for an 80-zone configuration [28]. Using more zones resulted in smoother pressure curves and HRR outcomes, which are particularly helpful for predicting burn duration.

Table 6 provides a concise comparison of UVATZ 4.0 with UVATZ 2.0 [30] and the University of Naples model [7]. This comparison highlights the shift from case-specific tuning to a systematic calibration procedure facilitated by a generalised HRF stratification approach. Additionally, the table outlines the trade-offs related to the chemistry approach, validation scope, fidelity proxy, and the accuracy achieved on the same engine platform. The chemistry-based approach requires more than twice the simulation time for a relatively coarse configuration. The fidelity of RCCI models is determined by the number of independent variables calculated, using the number of zones and their state properties. Chemical equations consume most of the computational resources. Disabling the chemistry in the boundary zones means UVATZ 4.0 offers lower fidelity than the previous version. Salahi et al. [32] showed simulation speeds up to 20 times faster by decoupling the chemistry step and solving it in parallel.

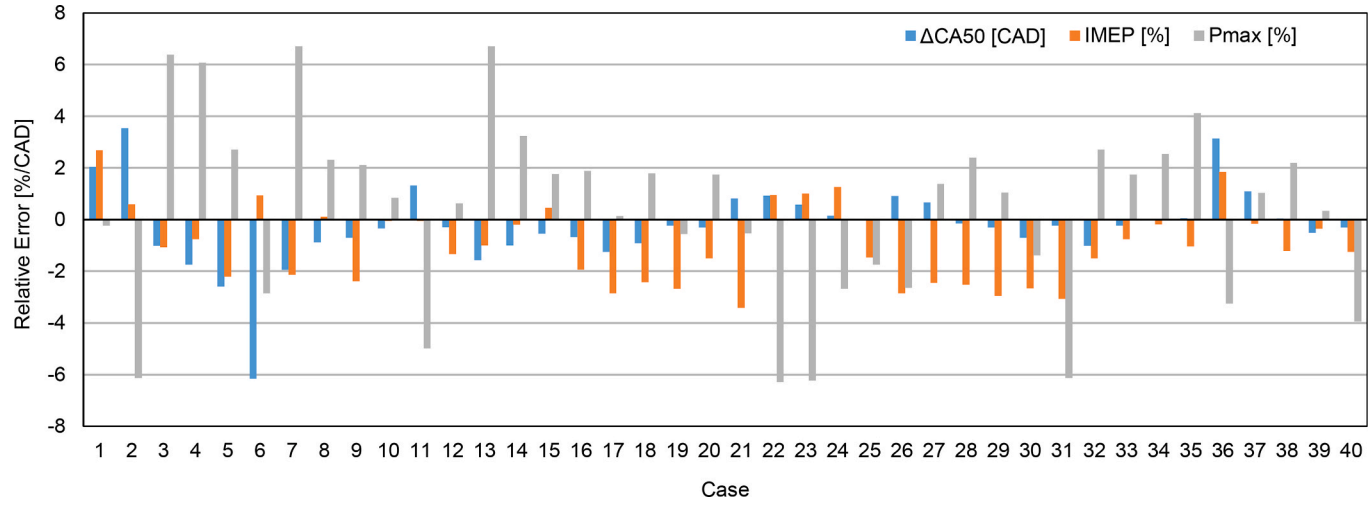

Fig. 16. Predicted IMEP and maximum pressure error with respect to experimental data for all cases.

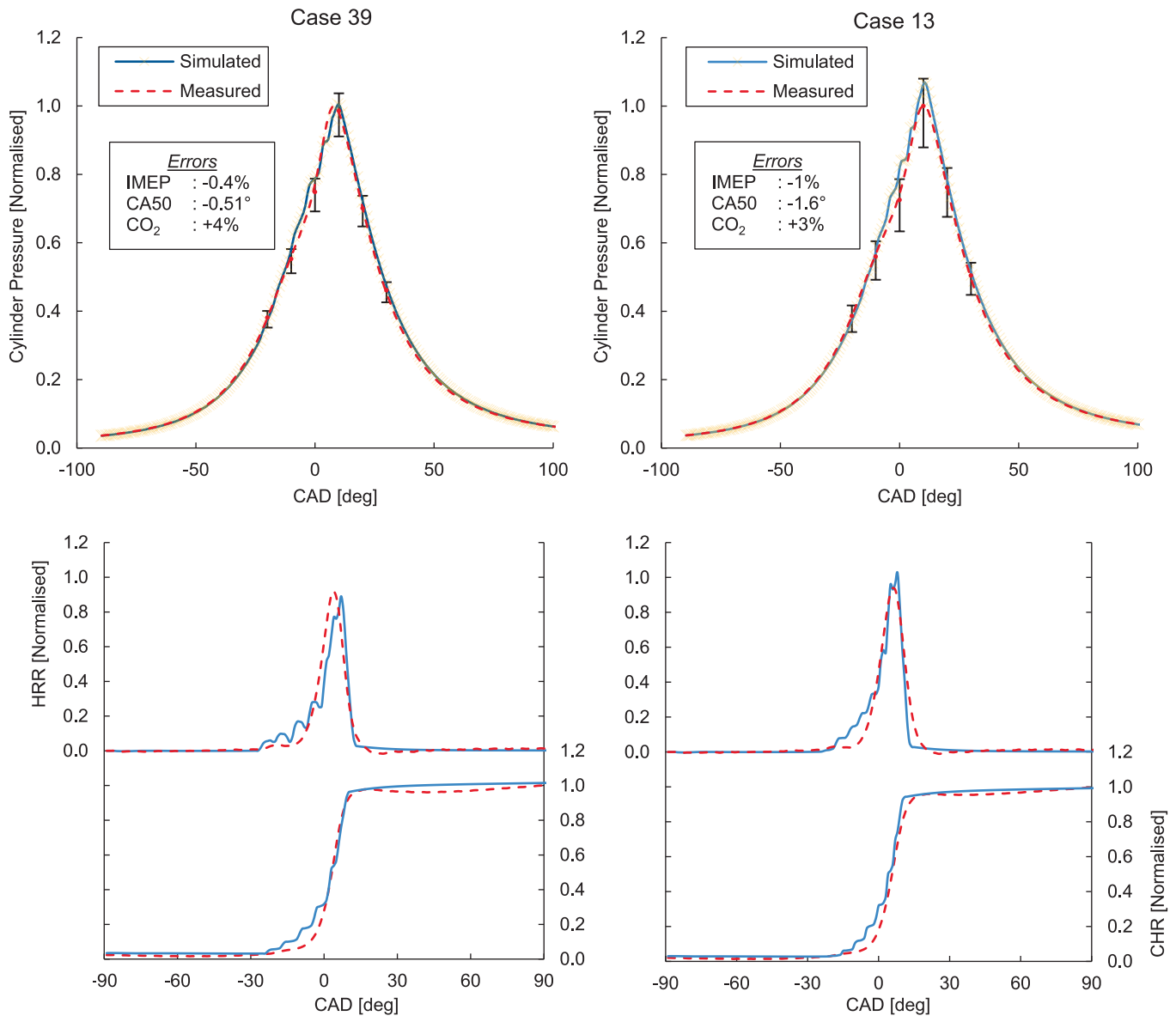

Fig. 17. Simulated pressure and CHR curves of two cases with the least and most maximum pressure error in comparison to the measured pressure.

Table 6
Benchmarking UVATZ 4.0 against other RCCI modelling approaches tested on the same Wärtsilä 31 engine platform.

	UVATZ 2.0 [30]	University of Naples [7]	UVATZ 4.0 (present study)
Chemistry	reduced-order (54 species)	tabulated	reduced-order (60 species)
Validation data	W31 (6 cases)	W31 (31 cases)	W31 (40 cases)
HRF-model	case-specific	empirical	semi-empirical
Peak pressure error	<4.5%	<12%	<7%
IMEP error	<2%	<5%	<4%
CA50 error	5 CAD	5 CAD	5 CAD
Fidelity (number of independent variables)	12×57 = 684	80×4 = 320	10×63 + 2×3 = 636
Calibration process	case-specific	engine-specific	engine-specific/ systematic

Although emission calibration was not included in this study, Vasudev et al. [5] showed that wall temperature and boundary layer assumptions significantly affected UHC and NOx formation. This means that precisely modelling the wall effect makes it possible to predict emissions without adding an external submodel. The key distinction of UVATZ compared to other reduced-order simulation approaches lies in its emphasis on phenomenon-oriented submodels rather than result-oriented ones. For example, flame propagation does not have to be implemented as before, since there is no conventional distinction of "burned/unburned" zones. Instead, it suffices to focus on the relevant gas dynamic phenomena related to flame propagation, such as mass continuity and momentum conservation. In this context, the object-oriented architecture of UVATZ allows flexible model extensions and enables users to choose the appropriate level of fidelity for any given simulation campaign. Shifting the engine simulation paradigm towards phenomena-oriented modelling further highlights the necessity and complexity of tuning methods. Therefore, the structured and step-by-step calibration process is another crucial outcome of the current study, serving as a key step in transitioning from the state of the science to the state of the art.

Table 6's HRF model trend suggests the HRF distribution is key to generalising the MZM for various operating conditions. Thus, the proposed beta distribution function can be identified as this studýs major

contribution, as it can capture the general form of HRF distribution. It effectively addresses the limitations of previous reduced-order models, which focused on the cone angle and penetration length, which are less relevant in RCCI cases with early injection and wall-affected spray. As shown in the results section, the validity of the findings is critically linked to β, which represents the fuel concentration near the wall.

The calibration framework is intentionally confined to a compact set of parameters with clearly separated roles: a single global reactivity multiplier, M, applied as a uniform chemical time-scale correction to compensate for mechanism and fuel-surrogate deficiencies without altering thermodynamic boundary conditions, and a beta-distribution-based HRF stratification model governed by (α, β), where α is treated as constant and β is represented through correlations in normalised operating descriptors (SOI, λ and blend ratio) rather than adjusted freely for each operating point. This design shifts calibration effort from operating-point-specific adjustments toward reusable relations across the operating map and reduces the effective degrees of freedom relative to earlier UVATZ implementations and other reduced-order approaches relying on multiple case-dependent tuning constants. Parameter transferability is therefore expected to be conditional: the stratification model is geometry-independent in formulation but may require re-identification when injector hardware, piston/bowl design, or the in-cylinder mixing field changes substantially, whereas the magnitude of M is primarily governed by the selected kinetic mechanism and fuel family and is thus more transferable across engines for a fixed CKM/fuel description than across different mechanisms or markedly different fuel chemistries.

At the same time, the beta-distribution approach represents an initial step toward a more phenomenology-driven spray description in RCCI simulation and still relies on statistical identification of its constants, which can limit extrapolation when operating conditions fall outside the calibration domain. Although the experimental campaign spans a wide set of operating points, it remains confined to a single engine platform (W31/SCRE); broader applicability is supported indirectly by the independent phenomenological verification of the stratification concept against external spray/CFD evidence and by consistent behaviour of the reactivity-scaling concept across alternative kinetic mechanisms, but dedicated multi-platform and multi-fuel validation remains a necessary next step. In this context, developing and integrating more explicit phenomenological spray models, extending the generalised chemistry assessment to a broader fuel set, and incorporating submodels for oil-induced pre-ignition and more detailed wall-component effects are logical steps toward a more rigorous and transferable simulation tool.

5. Conclusion

Using the University of Vaasa's advanced thermo-kinetic multi-zone model (UVATZ 4.0) as an implementation platform, the study shows that RCCI in large-bore marine engines can be simulated with high accuracy through structured reactivity adjustment and generalised fuel stratification modelling.

A key contribution is the transition from output-oriented parameter fitting towards a structured calibration philosophy. The introduction of a reactivity multiplier enables compensation for chemical-kinetic mechanism limitations, without disturbing thermodynamic boundary conditions. The consistent exponential dependence of the correction factor on premixed LRF concentration suggests that kinetic deficiencies can be handled systematically, rather than through case-by-case adjustment.

The introduced HRF stratification model, harnessing the beta distribution, demonstrates that physically meaningful fuel-distribution effects can be captured without reliance on CFD-derived inputs. Parameterising stratification using normalised SOI, λ, and blend ratio enables the framework to reduce calibration effort to a limited number of representative operating points, while maintaining high accuracy ($R^2 \approx 0.997$).

Key performance indicators were predicted within ±6% accuracy, without case-specific parameter adjustment. The maximum error in CA50 did not exceed 5 CAD for a single individual outlier (standard deviation ± 1 CAD). Importantly, the model inaccuracies were within cycle-to-cycle variations recorded in real engine operation. This combination of accuracy and predictivity compares favourably with best-in-class multi-zone models currently reported in the literature, where robustness depends on case-specific calibration or externally supplied fuel stratification data.

This combination narrows the gap between phenomenological understanding and practical application, enabling both systematic and knowledge-driven calibration of next-generation low-temperature combustion engines. Applicability is further strengthened through streamlined coupling with commercial engine-simulation platforms.

The balance between rapid calibration applications and deeper research-oriented analysis can be adjusted flexibly within the modular architecture by incorporating additional submodels. Future developments include, among others, predictive spray modelling, incorporation of flame-propagation components and detailed treatment of oil-induced pre-ignition and crevice-retained residuals.

Definitions/Abbreviations

BR	blend ratio
CA10/CA50	crank angle at 10%/50% mass burned
CAD	crank angle degree
CFD	computational fluid dynamics
CH_4	methane
CHR	cumulative heat release
CO_2	carbon dioxide
CKM	chemical kinetic mechanism
DF	dual-fuel
DNS	direct numerical simulation
EVO	exhaust valve opening
FEM	finite element method
GT-Suite	Gamma Technologies simulation suite
HRF	high-reactivity fuel
HRR	heat release rate
IMEP	indicated mean effective pressure
IVC	intake valve closing
LFO	light fuel oil
LHV	lower heat value
LRF	low-reactivity fuel
LTC	low-temperature combustion
MZM	multi-zone model
NG	natural gas
RCCI	reactivity-controlled compression ignition
RMS	root mean square
SOI	start of injection
SCRE	single-cylinder research engine
TDC	top dead centre
TEVC/TIVC	exhaust/intake valve closing time
TPA	three-pressure analysis
VVA	variable valve actuation
UHC	unburned hydrocarbons
UVATZ	University of Vaasa Advanced Thermo-kinetic multi-Zone
λ	lambda (air-fuel equivalence ratio)

$\dot{m}_{i\to j}$	mass transfer rate between zones
C_t	turbulence mixing intensity
D_w	diffusion factor
A	area/pre-exponential factor
δ_{ij}	central distance between zones i and j
ρ_i	density in zone i
r_n^+	non-dimensional radius
ζ_u	shear velocity coefficient
S_p	piston mean speed
μ_{wall}	wall viscosity
r	radius
R_{cyl}	cylinder radius
M	reactivity multiplier

(*continued on next page*)

(*continued*)

k_f	forward reaction rate constant
b	temperature exponent in Arrhenius equation
E_a	activation energy
R	global gas constant
T	temperature
f	fuel concentration function
$m_{injected}$	total injected fuel mass
$\overline{V}$	normalised cumulative volume (0 to 1)
a, b	spray start and end points
r_1, r_2	sensitivity exponents for spray distribution
C	normalisation constant
α, β	beta distribution shape parameters
$B(\alpha, \beta)$	beta function
P	pressure
Q	polynomial function for β modelling
$A_1 \cdots A_7$	coefficients in β polynomial model

CRediT authorship contribution statement

Kian Golbaghi: Writing – original draft, Visualization, Validation, Software, Methodology, Investigation, Formal analysis, Data curation, Conceptualization. **Hamidreza Maleki Almani:** Writing – original draft, Methodology, Formal analysis, Conceptualization. **Alireza Kakoee:** Supervision, Software, Conceptualization, Methodology. **Ben Smulter:** Writing – review & editing, Data curation, Methodology, Resources, Software. **Jari Hyvönen:** Supervision, Resources, Funding acquisition, Project administration. **Amin Andwari:** Writing – review & editing, Supervision, Resources, Project administration, Funding acquisition. **Maciej Mikulski:** Writing – review & editing, Writing – original draft, Supervision, Resources, Project administration, Methodology, Funding acquisition, Conceptualization.

Declaration of competing interest

The authors declare that they have no known competing financial interests or personal relationships that could have appeared to influence the work reported in this paper.

Acknowledgements

This study was funded by Business Finland as part of the CASEMATE Project (ref. 2911/31/2022). We would also like to appreciate Mr David Wilcox for his invaluable contribution in proofreading our manuscript and providing his expert suggestions on stylistic points.

Data availability

The data that has been used is confidential.

References

[1] Tay ZY, Konovessis D. Sustainable energy propulsion system for sea transport to achieve United Nations sustainable development goals: a review. Discov Sustain 2023;4:20. https://doi.org/10.1007/s43621-023-00132-y.
[2] Liu Y, Song E, Liu X. Scalable multi-fuel control system architecture for marine internal combustion engine. In: Yang D, editor. 2023 International conference on marine equipment & technology and sustainable development. Singapore: Springer Nature Singapore; 2023. p. 1176–87.
[3] Kuittinen N, Heikkilä M, Jalkanen J-P, Aakko-Saksa P, Lehtoranta K. Methane slip emissions from LNG vessels -review, 2023.
[4] Singh AP, Kumar V, Agarwal AK. Evaluation of comparative engine combustion, performance and emission characteristics of low temperature combustion (PCCI and RCCI) modes. Appl Energy 2020;278:115644. https://doi.org/10.1016/j.apenergy.2020.115644.
[5] Vasudev A, Kakoee A, Axelsson M, Almani HM, Hyvönen J, Mikulski M. Advancing autonomy of chemical kinetics based multizone models for reactivity controlled compression ignition engines. Energ Conver Manage 2024;312:118562. https://doi.org/10.1016/j.enconman.2024.118562.
[6] Joseph M, Ismail S, Jothi TJS. Effect of compression ratio and hydrogen addition on performance and different phases of hydrogen/diesel combustion in reactivity controlled compression ignition engine. Clean Energy 2025;9:46–61. https://doi.org/10.1093/ce/zkae119.
[7] De Felice M, De Bellis V, Malfi E, Gambardella A, Bozza F, Cafari A, et al. A novel phenomenological model for stratification-controlled low temperature combustion applied to a dual-fuel marine internal combustion engine supplied with natural gas and light fuel oil. Fuel 2025;386:134218. https://doi.org/10.1016/j.fuel.2024.134218.
[8] Asadollahzadeh P, Hamedi MH, Jazayeri SA. A comprehensive study of a reactivity-controlled compression ignition engine fueled with biogas and diesel oil. Clean Techn Environ Policy 2021;23:113–26. https://doi.org/10.1007/s10098-020-01983-z.
[9] Jin T, Wu Y, Wang X, Luo KH, Lu T, Luo K, et al. Ignition dynamics of DME/methane-air reactive mixing layer under reactivity controlled compression ignition conditions: Effects of cool flames. Appl Energy 2019;249:343–54. https://doi.org/10.1016/j.apenergy.2019.04.161.
[10] Mikulski M, Balakrishnan PR, Hunicz J. Natural gas-diesel reactivity controlled compression ignition with negative valve overlap and in-cylinder fuel reforming. Appl Energy 2019;254:113638. https://doi.org/10.1016/j.apenergy.2019.113638.
[11] Pachiannan T, Zhong W, Rajkumar S, He Z, Leng X, Wang Q. A literature review of fuel effects on performance and emission characteristics of low-temperature combustion strategies. Appl Energy 2019;251:113380. https://doi.org/10.1016/j.apenergy.2019.113380.
[12] Premkumar A, Loffredo F, Pitsch H, Klein M. Towards direct numerical simulations of reactivity-controlled compression ignition engine using n-octanol/ethanol fuel blends. Flow Turbul Combust 2025;115:275–301. https://doi.org/10.1007/s10494-024-00570-2.
[13] Halis S, Solmaz H, Polat S, Yücesu H. Numerical investigation of a reactivity-controlled compression ignition engine fueled with N-heptane and iso-octane. Sustainability 2023;15:10406. https://doi.org/10.3390/su151310406.
[14] Dwarshala SK, Rajakumar SS, Kummitha OR, Venkatesan EP, Veza I, Samuel OD. A review on recent developments of RCCI engines operated with alternative fuels. Energies 2023;16. https://doi.org/10.3390/en16073192.
[15] Paykani A, Garcia A, Shahbakhti M, Rahnama P, Reitz RD. Reactivity controlled compression ignition engine: Pathways towards commercial viability. Appl Energy 2021;282:116174. https://doi.org/10.1016/j.apenergy.2020.116174.
[16] Yadav J, Günther M, Pischinger S. Optical spray investigation and numerical spray model calibration for the RCCI combustion mode with ethanol/CNG and diesel fuel. Energ Conver Manage 2024;302:118159. https://doi.org/10.1016/j.enconman.2024.118159.
[17] Kakoee A, Golbaghi K, Cafari A, Vasudev A, Mehranfar S, Andwari AM, et al. The interplay between combustion and component thermal loading in next-generation marine engines employing reactivity-controlled compression ignition. Energies 2025;19:83. https://doi.org/10.3390/en19010083.
[18] Zhou D, Yang W, Zhao F, Li J. Dual-fuel RCCI engine combustion modeling with detailed chemistry considering flame propagation in partially premixed combustion. Appl Energy 2017;203:164–76. https://doi.org/10.1016/j.apenergy.2017.06.021.
[19] Franken T, Matrisciano A, Sari R, Fogué Robles Á, Monsalve-Serrano J, Lopez Pintor D, et al. Modeling of reactivity controlled compression ignition combustion using a stochastic reactor model coupled with detailed chemistry, 2021, p. 2021-24–0014. doi: 10.4271/2021-24-0014.
[20] Vasudev A, Mikulski M, Balakrishnan PR, Storm X, Hunicz J. Thermo-kinetic multi-zone modelling of low temperature combustion engines. Prog Energy Combust Sci 2022;91:100998. https://doi.org/10.1016/j.pecs.2022.100998.
[21] Bai X-S. Numerical simulation of turbulent combustion in internal combustion engines. In: De S, Agarwal AK, Chaudhuri S, Sen S, editors. Modeling and Simulation of Turbulent Combustion. Singapore: Springer Singapore; 2018. p. 513–41. https://doi.org/10.1007/978-981-10-7410-3_17.
[22] Egüz U, Maes NCJ, Leermakers CAJ, Somers LMT, Goey LPHD. Predicting auto-ignition characteristics of RCCI combustion using a multi-zone model. Int J Automot Technol 2013;14:693–9. https://doi.org/10.1007/s12239-013-0075-2.
[23] Eichmeier JU, Reitz RD, Rutland C. A zero-dimensional phenomenological model for RCCI combustion using reaction kinetics. SAE Int J Engines 2014;7:106–19. https://doi.org/10.4271/2014-01-1074.
[24] Hiroyasu H, Kadota T, Arai M. Development and use of a spray combustion modeling to predict diesel engine efficiency and pollutant emissions : Part 1 combustion modeling. Bull JSME 1983;26:569–75. https://doi.org/10.1299/jsme1958.26.569.
[25] Mikulski M, Bekdemir C, Willems F. Experimental validation of a combustion kinetics based multi-zone model for natural gas-diesel RCCI. Engines 2016.
[26] Mikulski M, Bekdemir C. Understanding the role of low reactivity fuel stratification in a dual fuel RCCI engine – A simulation study. Appl Energy 2017;191:689–708. https://doi.org/10.1016/j.apenergy.2017.01.080.
[27] Raza M, Wang H, Yao M. Numerical investigation of reactivity controlled compression ignition (RCCI) using different multi-component surrogate combinations of diesel and gasoline. Appl Energy 2019;242:462–79. https://doi.org/10.1016/j.apenergy.2019.03.115.
[28] De Bellis V, Malfi E, Lanotte A, Fasulo G, Bozza F, Cafari A, et al. Development of a phenomenological model for the description of RCCI combustion in a dual-fuel marine internal combustion engine. Appl Energy 2022;325:119919. https://doi.org/10.1016/j.apenergy.2022.119919.
[29] Vasudev A, Cafari A, Axelsson M, Mikulski M, Hyvonen J. Towards next generation control-oriented thermo-kinetic model for reactivity controlled compression ignition marine engines. SAE Techn Pap 2022. https://doi.org/10.4271/2022-01-1033.
[30] Kakoee A, Vasudev A, Smulter B, Hyvonen J, Mikulski M. A predictive 1D modeling framework for reactivity-controlled compression ignition engines, via a chemistry-

based, multizone combustion object. In: 16th international conference on engines & vehicles, SAE International; 2023. https://doi.org/10.4271/2023-24-0001.
[31] Mikulski M, Ovaska T, Rabetino R, Kangasjärvi M, Myllykangas A. Clean propulsion technologies: securing technological dominance for the finnish marine and off-road powertrain sectors. Energies 2025;18:1240. https://doi.org/10.3390/en18051240.
[32] Salahi MM, Moradi J, Golbaghi K, Heidarabadi S, Andwari A, JariHyvönen, et al. A novel parallel solver using decoupled chemical–physical integration for rapid multizone simulation of reactivity controlled combustion in engines. Energy Convers Manage: X 2026:101865. doi: 10.1016/j.ecmx.2026.101865.
[33] Nazemi M, Shahbakhti M. Modeling and analysis of fuel injection parameters for combustion and performance of an RCCI engine. Appl Energy 2016;165:135–50. https://doi.org/10.1016/j.apenergy.2015.11.093.
[34] Kakoee A, Mikulski M, Vasudev A, Axelsson M, Hyvönen J, Salahi MM, et al. Start of injection influence on in-cylinder fuel distribution, engine performance and emission characteristic in a RCCI marine engine. Energies 2024;17. https://doi.org/10.3390/en17102370.
[35] Yao T, Pei Y, Zhong B-J, Som S, Lu T, Luo KH. A compact skeletal mechanism for n-dodecane with optimized semi-global low-temperature chemistry for diesel engine simulations. Fuel 2017;191:339–49. https://doi.org/10.1016/j.fuel.2016.11.083.
[36] Salahi MM, Andwari AM, Kakoee A, Golbaghi K, Hyvönen J, Gharehghani A, et al. New chemical kinetics mechanism for simulation of natural gas/hydrogen/diesel multi-fuel combustion in engines, 2025. doi: 10.3384/ecp212.048.
[37] Goodwin DG, Speth RL, Moffat HK, Weber BW. Cantera: An object-oriented software toolkit for chemical kinetics, thermodynamics, and transport processes 2021. doi: 10.5281/zenodo.4527812.
[38] Goodwin DG, Moffat HK, Schoegl I, Speth RL, Weber BW. Cantera: an object-oriented software toolkit for chemical kinetics, thermodynamics, and transport processes 2024. doi: 10.5281/ZENODO.14455267.
[39] Chang J, Güralp O, Filipi Z, Assanis DN, Kuo T-W, Najt P, et al. New heat transfer correlation for an HCCI engine derived from measurements of instantaneous surface heat. Flux 2004. https://doi.org/10.4271/2004-01-2996.
[40] Yang J, Martin JK. Approximate solution—one-dimensional energy equation for transient, compressible, low Mach number turbulent boundary layer flows. J Heat Transfer 1989;111:619–24. https://doi.org/10.1115/1.3250727.
[41] Bozza F, Teodosio L, De Bellis V, Fontanesi S, Iorio A. A refined 0D Turbulence Model To Predict Tumble And Turbulence In SI engines. SAE Int J Engines 2018;12:15–30. https://doi.org/10.4271/03-12-01-0002.
[42] Cohen SD, Hindmarsh AC, Dubois PF. CVODE, A stiff/nonstiff ODE solver in C. Comput Phys 1996;10:138–43. https://doi.org/10.1063/1.4822377.
[43] Gamma technologies. GT-POWER 2024.
[44] Sandia National Laboratories. Sandia Spray M Data. Engine Combustion Network - Spray M n.d. https://ecn.sandia.gov/data/sandia-spray-m-data/ (accessed December 2, 2025).
[45] Binet JPM. Mémoire sur les intégrales définies eulériennes: et sur leur application à la théorie des suites, ainsi qu' à l'évaluation des fonctions grands nombres. Editeur non identifié; 1839.
[46] Jay, D. CR development in the last decade in Wärtsilä. 28th CIMAC world congress, Helsinky, Finland, 2016, p. 6–10.
[47] A.J. Martyr, M.A. Plint. Engine testing, theory and practice. Elsevier; 2007. doi: 10.1016/B978-0-7506-8439-2.X5000-2.
[48] Vlaswinkel M, Willems F. Data-based in-cylinder pressure model with cyclic variations for combustion control: an RCCI engine application. Energies 2024;17:1881. https://doi.org/10.3390/en17081881.
[49] Heywood J. Internal combustion engine fundamentals 2E. McGraw Hill LLC; 2018.
[50] Tekgül B, Kahila H, Karimkashi S, Kaario O, Ahmad Z, Lendormy É, et al. Large-eddy simulation of spray assisted dual-fuel ignition under reactivity-controlled dynamic conditions. Fuel 2021;293:120295. https://doi.org/10.1016/j.fuel.2021.120295.
[51] Hunicz J, Yang L, Ji S, Mikulski M. An experimental study on the coupling effect of swirl ratio and injection timing in reactivity-controlled compression ignition gas engines. (Under Review) 2026.
[52] Hockett A, Hampson G, Marchese AJ. Development and validation of a reduced chemical kinetic mechanism for computational fluid dynamics simulations of natural gas/diesel dual-fuel engines. Energy Fuels 2016;30:2414–27. https://doi.org/10.1021/acs.energyfuels.5b02655.
[53] Combustion n.d. https://combustion.llnl.gov/ (accessed January 2, 2026).